

High-dimensional optimal design of dual-rotor synchronous reluctance machines based on data-driven torque decomposition

Farnam Farshbaf-Roomi¹  | Aran Shoaee¹  | Jianguo Zhu² | Qingsong Wang¹

¹Département de génie électrique, École de technologie supérieure (ÉTS), Montreal, Quebec, Canada

²School of Electrical and Information Engineering, University of Sydney, Sydney, New South Wales, Australia

Correspondence

Qingsong Wang.
Email: qingsong.wang@etsmtl.ca

Funding information

Natural Sciences and Engineering Research Council of Canada

Abstract

The multi-objective optimal design of double-sided stator dual-rotor synchronous reluctance machines (DSS-DRSynRMs) is a challenging high-dimensional problem. The objective of this paper is to present a new optimal design method based on data-driven models and the principle of torque decomposition addressing the aforementioned issue. For this purpose, a 26-parameter optimisation problem is solved by employing the proposed method consisting of three sequential phases. Through the proposed method, the combination of artificial neural network (ANN) and recently introduced waveform targeting surrogate model (WTSM) strategy is investigated to mitigate the computational complexity of the optimisation process. Furthermore, the electromagnetic performance of the final optimal design has been comprehensively analysed showing a significant reduction in torque ripple rate and improved torque density. Moreover, the computational efficiency of the proposed method has been compared to the popular multi-level multi-objective optimisation method. From the discussion, it can be found that the proposed method provides a reduced computation time and wider search space.

KEYWORDS

optimisation, synchronous motors

1 | INTRODUCTION

With the global push towards vehicle electrification, there is a growing need for high-performance electric machines, particularly in traction applications. Meeting the demands for high continuous and peak torque density, superior efficiency, and a broad constant power speed range has pushed machine designers to explore new frontiers. Among the promising innovations are double airgap radial flux machines (DAMs), which are typically composed of multiple stators or rotors, unlike single rotor/stator machines or magnetically geared machines. DAMs offer the potential for significantly higher power density, making them a compelling alternative in the quest for optimised electric machine performance [1, 2].

The dual-rotor machines (DRMs) are considered a subcategory of DAMs where each rotor can operate independently or both rotors can be integrated to a single load [3]. The stator of these machine on the other hand, can consist of double-sided

(DSS-DRM) configuration or yokeless stator structure (YS-DRM). The DSS-DRM features a design where the inner and outer stator teeth share a common back iron, while the YS-DRM has a configuration with single parallel stator teeth. While the YS-DRMs can provide a lighter design due to absence of the stator yoke, the DSS-DRMs experience more robust structure and easier design-to-manufacture process [4, 5].

With respect to the advantages of DSS-DRMs in proposing robust and high torque density machines, its potential application in synchronous reluctance machines (SynRMs) has been a matter of rising interest on recent research [6, 7]. The simple rotor structure, low cost and relatively low-torque ripple makes them a good candidate for variety of applications including transportation. Therefore, the design and optimisation of the double-sided stator dual-rotor SynRM (DSS-DRSynRM) is going to be discussed in this paper.

The optimal design of DSS-DRSynRM requires a more detailed process development due to increased size of number

This is an open access article under the terms of the [Creative Commons Attribution-NonCommercial-NoDerivs](https://creativecommons.org/licenses/by-nc-nd/4.0/) License, which permits use and distribution in any medium, provided the original work is properly cited, the use is non-commercial and no modifications or adaptations are made.

© 2025 The Author(s). *IET Electric Power Applications* published by John Wiley & Sons Ltd on behalf of The Institution of Engineering and Technology.

of effective design variables compared to conventional SynRM. Therefore, the need for adoption of a reliable and computationally efficient optimisation method is an essential to find the best solution. Finite element model (FEM) is the most accurate computation method for performance estimation of electrical machines in all sizes and applications [8–10]. However, due to the high-dimensional nature of the optimisation problem of DSS-DRSynRMs, direct search will be very time consuming. Even with the recent advances in the computer hardware, it is not affordable to apply direct search based on FEM. To address this problem, data-driven modelling techniques have gained a significant interest in recent years [11–14].

Data-driven models are tools to replace FEM in order to predict the performance of the electrical machines in the optimisation process. However, special attention must be applied to construct a reliable model in terms of both accuracy and computational cost. In general, combination of a proper initial sampling approach can effectively improve the accuracy and computational efficiency of the data-driven model. Various sampling methods such as the Latin hypercube sampling (LHS), full factorial (FF) test, central composite design and Box–Behnken method are available to increase the efficiency of the model construction [15, 16]. However, the sampling method alone would not be sufficient since an adequate fitting method to train the data-driven model is crucial. In this regard, advanced fitting methods such as kriging, radial basis function (RBF) and artificial neural network (ANN) are widely utilised in variety of optimisation problems [17–19].

The key contribution of this paper is to propose a new optimal multi-objective design method for DSS-DRSynRMs based on surrogate models. For this purpose, this paper utilises the newly introduced waveform-targeted surrogate modelling (WTSM) strategy [20]. The WTSM strategy is responsible to predict the important waveforms such operating torque, cogging torque or back electromotive (EMF). This feature helps to change the focus of surrogate modelling from optimisation targets such as average torque, torque ripple or total harmonic distortion (THD) of back EMF to the waveforms which are the main source of these objective functions. The main advantage of WTSM is the capability of eliminating undesired post-processing effect on the training datasets which consequently increases the accuracy of the surrogate modelling process. Therefore, this method is fundamentally different from conventional data-driven optimisation models leading to a significant reduction in computational cost while the accuracy of the surrogate models is improved. The presented work is organised as follows: first, the initial design and the multi-objective optimisation problem alongside 26 design parameters is discussed in section 2. In section 3, the detailed description of the proposed WTSM-based optimisation model is presented. The section consists of three sequential phases namely: torque decomposition, ANN-based WTSM and multi-objective optimisation. Finally in section 4, the performance of the obtained optimal solution is analysed and compared to the initial design. In addition, the computational efficiency of the proposed method is compared to the popular multi-level optimisation method.

2 | DESIGN SPECIFICATIONS AND MULTI-OBJECTIVE OPTIMISATION PROBLEM DEFINITION

As mentioned earlier, this paper aims to provide a new surrogate-assisted optimisation solution for optimal design of DSS-DRSynRMs. In this regard, an example benchmark design is selected. Figure 1 illustrates the topology of studied machine. As can be seen, the winding configuration is defined as two mirrored slots are connected to reduce the end winding length and copper loss [7]. Table 1 also shows the design specifications for the machine optimisation.

Figure 2 illustrates the flux density in the initial machine due to D-axis and Q-axis excitation with maximum available current respectively. As can be seen, the flux lines coming from

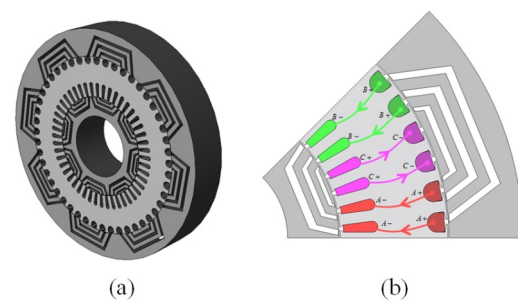


FIGURE 1 DSS-DRSynRM topology (a) 3D view of core (b) Winding configuration based on Ref. [7].

TABLE 1 Design specifications of DSS-DRSynRM.

Parameter	Description	Value
I_c	Coil current	70 (A)
p	Number of poles	8
S	Number stator slots	96 (2*48)
N_{tc}	Turn per coil	6
RPM	Mechanical speed	200 (rpm)
g	Airgap length	0.75 (mm)
L_{stk}	Core stack length	80 (mm)
D_{in}	Inner rotor diameter	194.4 (mm)
D_{out}	Outer rotor diameter	347.84 (mm)

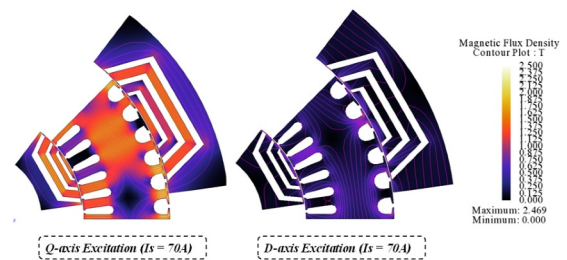


FIGURE 2 Magnetic flux density distribution with D-axis and Q-axis excitations.

each side of the stator are circulating over the rotor and the stator yoke. Therefore, the stator yoke's flux density is dependent on both the magnetic circuits located in each side of the stator. To prevent any magnetic saturation in the stator's yoke, a proper analytical sizing and FEM-based tuning have been applied into the initial design stage.

The initial design stage is always necessary to find a good starting point for finding an optimum solution for the specified design requirements. However, to maximise the performance factors of the machine, a multi-objective optimisation process is vital. Therefore, the studied problem is defined as follows:

$$\begin{cases} \text{Max } T_{ave} \\ \text{Min } T_{rip}(\%) \\ \text{Cons}_{Torque} : [T_{ave} > 86\text{Nm}] \\ \text{Cons}_{kg} : [\text{Weight} < 70 \text{kg}] \end{cases} \quad (1)$$

where T_{ave} and $T_{rip}(\%)$ are average output torque and the ripple rate, respectively. Also, two additional constraints have been defined to narrow down the search space. For the optimisation process, various geometrical parameters are existing on the inner rotor, outer rotor and the stator.

In DSS-DRSynRMs with unsaturated yoke, the analytical electromagnetic torque can be simply described as combination of two rotors generating torques:

$$T_e = \frac{3}{2} p (L_{d_{inner}} - L_{q_{inner}} + L_{d_{outer}} - L_{q_{outer}}) i_d i_q \quad (2)$$

where $L_{d_{inner}}, L_{q_{inner}}, L_{d_{outer}}$ and $L_{q_{outer}}$ are the DQ-inductances for inner and outer rotors respectively. Therefore, by having a constant magnetomotive force (MMF), it is possible to optimise the torque profile based on the rotor parameters dependent to the fixed stator structure. For this purpose, 26 variables have been defined to parametrically investigate various rotor configurations (see Figure 3).

As can be seen, the large number of design parameters indicates a high-dimensional optimisation problem. Therefore, a comprehensive sensitivity analysis is necessary to quantitatively

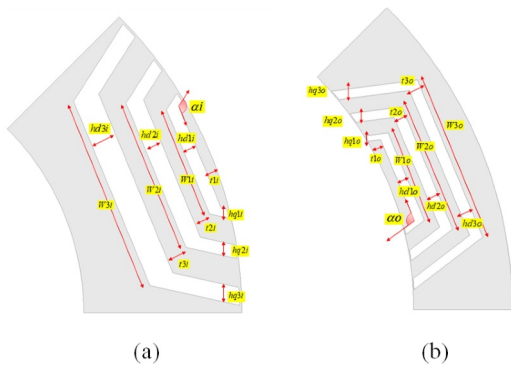


FIGURE 3 Design parameters (a) inner rotor and (b) outer rotor.

analyse the influence of different design variables on the objectives before initiating the surrogate-based optimisation. For this purpose, the Pearson correlation coefficient analysis method is utilised where each coefficient can be calculated as follows:

$$\rho_{X_i, Y_i} = \frac{N \sum X_i Y_i - \sum X_i \sum Y_i}{\sqrt{N \sum X_i^2 - (\sum X_i)^2} \sqrt{N \sum Y_i^2 - (\sum Y_i)^2}} \quad (3)$$

Figure 4 presents the absolute value of the coefficients corresponding to the relation of each design parameter with the measured objective functions based on the Taguchi orthogonal array with 3 levels (L108) applied to the Table 2. The measured values demonstrate that some of the design parameters have a relatively strong linear effect on T_{ave} .

Meanwhile, the corresponding coefficients for $T_{rip}(\%)$ are following a weak linear behaviour. This observation indicates the existence of a sensitive relation between $T_{rip}(\%)$ and all of the 26 input variables. Therefore, neglecting one or multiple design variables from design space could harm the effective search space.

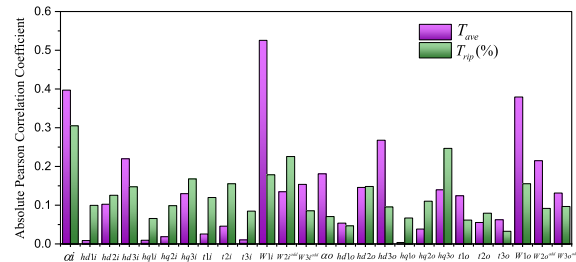


FIGURE 4 Pearson correlation coefficients on DSS-DRSynRM's design parameters.

TABLE 2 Initial value and range for design parameters.

Var.	Initial	Range	Var.	Initial	Range
a_i	125	[105,125]	a_o	105	[105,115]
$bd1_i$	3 mm	[1,3]	$bd1_o$	5 mm	[1,6]
$bd2_i$	4 mm	[1,4]	$bd2_o$	6 mm	[1,6]
$bd3_i$	6 mm	[2,6]	$bd3_o$	6 mm	[2,7.2]
$bq1_i$	2 mm	[0.5,2]	$bq1_o$	3 mm	[1,3]
$bq2_i$	3 mm	[1,3]	$bq2_o$	5 mm	[2,5]
$bq3_i$	4 mm	[1,4]	$bq3_o$	5 mm	[2,5]
$t1_i$	2 mm	[1,2]	$t1_o$	5 mm	[1.5,5]
$t2_i$	4 mm	[1,4]	$t2_o$	6 mm	[3,6]
$t3_i$	5 mm	[2,5]	$t3_o$	7 mm	[4,7]
$W1_i$	13 mm	[5,13]	$W1_o$	25 mm	[15,26]
$W2_i^{add}$	5 mm	[2,5]	$W2_o^{add}$	10 mm	[5,13]
$W3_i^{add}$	5 mm	[2,5]	$W3_o^{add}$	10 mm	[5,10]

3 | PROPOSED WTSM-BASED OPTIMISATION MODEL

The torque profile features namely the average torque and torque ripple rate are one of the main optimisation targets as in all the electric motors. In this work, to optimally design a DSS-DRSynRM, a new data-driven optimisation method based on WTSM is presented. Figure 5 illustrates the flowchart of the proposed optimisation process. The detailed description of each step is described as follows:

3.1 | Phase1: Torque decomposition

In the first phase of the proposed optimisation method, the proper initial design of the DSS-DRSynRM must be accomplished through an iterative tuning process. While the machine torque depends on the airgap diameter of each rotor, the saturation level of stator yoke plays a decisive role on determining the effective airgap flux density. Figure 6 illustrates the variation of the stator yoke flux density (B_{sy}) with respect to the yoke's width (wsy). As can be seen, a low value of ' wsy ' will result in highly saturated machine and consequently, the effective flux in the airgap will significantly reduce. Another deficit of a thin stator yoke in DSS-DRSynRM is the reduction of airgap diameter of outer rotor (D_{yro}) which will provide a lower torque value with the fix amount of shear maxwell. On the other hand, uncontrolled increase of yoke width will increase the material cost and weight of the machine. Therefore, a suitable operation point ($B_{sy} \leq 1.55T$) is selected to match with the desired operation characteristics.

As mentioned in previous section, the studied multi-objective optimisation problem includes 26 design parameters distributed in both rotor sides. In the case of utilising conventional data-driven model-assisted optimisation techniques presented in previous research, a specific surrogate model should be assigned to each objective that can accurately predict the input–output relation in the studied problem. However, this approach will require a significantly large number of FEM simulation to generate an appropriate number of samples and proper accuracy in the predicted output values. For example, by considering only 3 levels for each parameter in FF-based sampling method and data, the training dataset will contain 3^{26} samples which is computationally unaffordable. Other option is using methods such as multi-level optimisation where the search space must be divided to multiple levels. However, this will result in a smaller search space, multiple iterations and possible loss of the real optimum solutions. To tackle these issues, this work takes advantage of the decomposability of the torque waveform of the DSS-DRSynRMs. As it is illustrated in Figure 7, the generated output torque of the machine is the sum of torque produced by each rotor segment. By analysing the magnetic equivalent circuit (MEC) of the machine, it is evident that the inner rotor airgap flux (ϕ_i) and outer rotor airgap flux (ϕ_o) is dependent to the variable magnetic reluctance of stator's yoke (R_{js}) where the reluctance

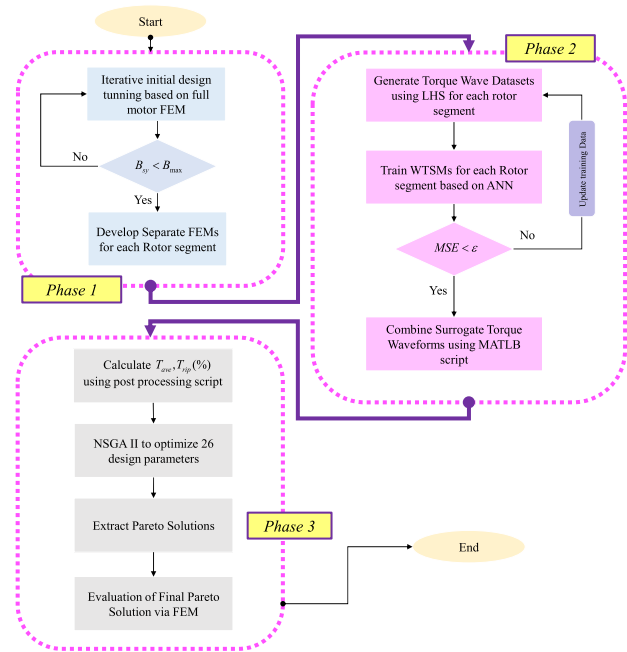


FIGURE 5 Flowchart of the proposed WTSM-based optimisation.

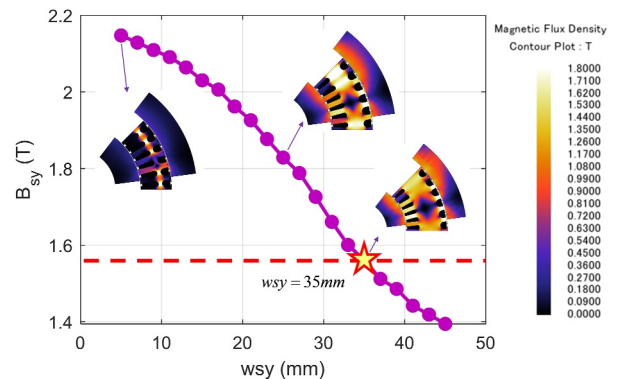


FIGURE 6 Effect of stator yoke width (wsy) on its flux density (B_{sy}).

value depends on B_{sy} . Therefore, the stator's yoke will behave as a magnetic short-circuit path due the proper selection of stator's yoke width (wsy). Consequently, ϕ_i and ϕ_o can be determined separately from each other. The latter helps to individually model each rotor side's torque waveform and to eliminate the cross-coupling between design parameters located on inner rotor and outer rotor. In this regard, models can be constructed with 13 variables instead of 26 variables.

Although the torque waveform decomposition will eliminate the cross-coupling effect, the value of objectives such as $T_{rip}(\%)$ still depends directly on both rotor dimensions simultaneously. This dependency can be described using Equations (4) and (5):

$$\begin{aligned} T_{ave} &= \frac{1}{\tau} \int T_{total}(t) dt = \frac{1}{\tau} \int (T_{inner}(t) + T_{outer}(t)) dt \\ &= T_{ave_{inner}} + T_{ave_{outer}} \end{aligned} \quad (4)$$

$$T_{rip}(\%) = \frac{\max(T_{total}(t)) - \min(T_{total}(t))}{T_{ave}} \neq T_{rip}(\%)_{inner} + T_{rip}(\%)_{outer} \quad (5)$$

As it is written in Equation (4), T_{ave} can be calculated based on combining the average torque of inner and outer rotors which they are only the function the design parameters located on the corresponding rotor segment. However, as it is described in Equation (5), $T_{rip}(\%)$ still depends on both of the rotor segments despite of the decomposability of the torque waveforms. Consequently, 26 design parameters still are needed to construct the surrogate model for torque ripple.

To address this issue, this paper uses a newly proposed WTSM method which is responsible to prediction of waveforms instead of single-output values. In other words, the WTSM will separately compute the torque waveform of each rotor segment and as a result, the number of variables for data-driven model construction will decrease to 13 helping to significantly reduce the computational cost. Figure 8 illustrates the concept of WTSM-based prediction of waveform-related objectives such as average torque and torque ripple. As can be seen, with the assist of torque decomposition and WTSM, 26 variables can be connected to the outputs while only 13 variables are needed to be considered in each training and surrogate model construction process. The detailed description of the WTSM strategy can be found in Ref. [20] for further reading.

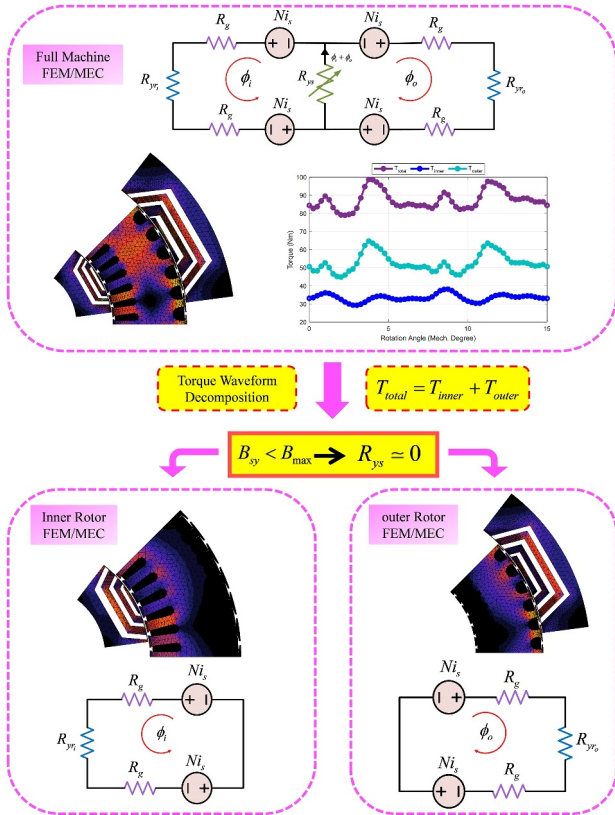


FIGURE 7 Principle of torque waveform decomposition in DSS-DRSynRM with respect of MEC.

3.2 | Phase2: ANN-based WTSM

To develop an accurate group of data-driven required for WTSM strategy, two important factors must be considered. First the effect of number of variables which is 13 in each WTSM model. The second is the fitting method to construct the models in each evaluated time step. The latter can vary the prediction accuracy of the trained models with respect to a fixed training dataset. To find pareto optimum solutions for the studied multi-objective optimisation problem, this paper implements the combination of the LHS method with ANN-based WTSM. Due to high-dimensional nature of the DSS-DRSynRM, the adopted sampling approach and model training methods are proven to be superior options. With respect to the obtained sensitivity analysis results and the torque decomposition approach, 1000 samples for T_{inner} and 4000 samples for T_{outer} were generated to create training-validation datasets. For accurately modelling the torque waveforms, each rotor segment must rotate 60 electrical degrees. Therefore, 61 steps have been considered to measure instantaneous torque. Based on collected torque waveform data, an ANN model has constructed for each time step. In this regard, 122 ANN models (61 model each) have been established to predict the torque waveform with respect to the input variables. Figure 9 shows the accuracy of ANN models constructed for step (1), step (31) and step (61). An example of ANN-based WTSM is presented in Figure 10, which compares the torque waveform of inner and outer rotors of the initially designed DSS-DRSynRM. As can be seen, an acceptable agreement has been achieved with prediction of T_{inner} and T_{outer} .

To comprehensively analyse the effect of utilising ANN models to construct WTSMs, the measured accuracy metrics have been compared to the Kriging model-based WTSM in

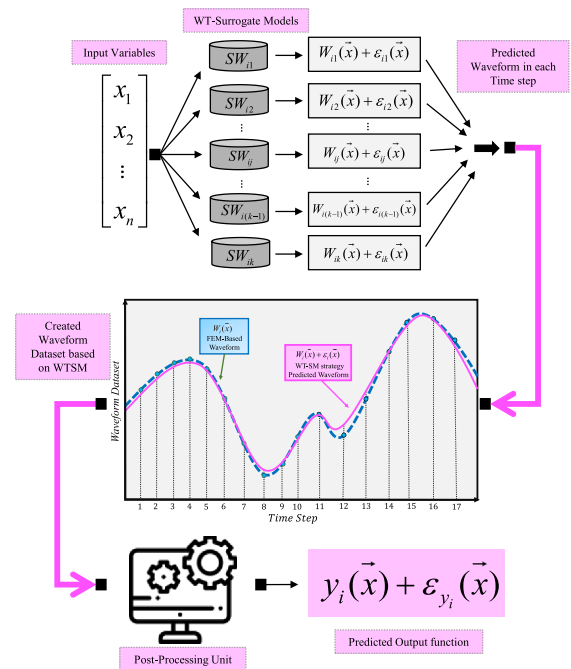


FIGURE 8 Conceptual visualisation of WTSM strategy [20].

Figure 11. The Kriging modelling technique is a spatial distance-based interpolation method that uses variograms to estimate local and global structure of objective functions which is widely used in electrical machine applications. An inherently similar approach is also can be found in the RBF surrogate modelling method. Therefore, the

Kriging method has been chosen for further accuracy comparisons. As it is evident, the Kriging method failed to perform while the ANN method was able to provide a high accuracy with the same training and validation datasets. This results also proves the capability of ANN modelling for tackling high-dimensional problems.

3.3 | Multi-objective optimisation

With the help of constructed WTSMs, the T_{ave} and $T_{rip}(\%)$ can be calculated using post-processing script combining T_{inner} and T_{outer} and applying mathematical formulae. Moreover, it is possible to fully investigate the design space with 26 variables and find the best pareto solutions. For this

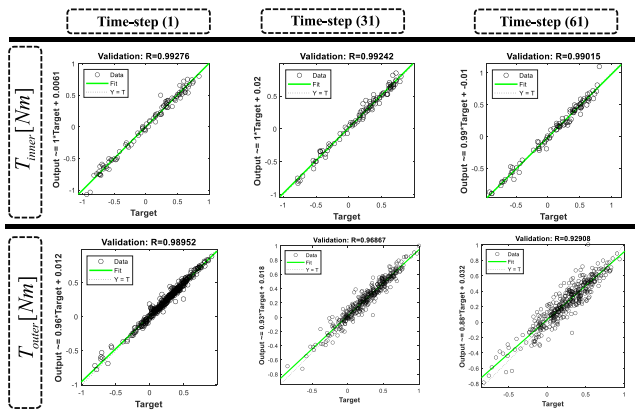


FIGURE 9 Accuracy analysis for trained ANNs on Step 1, step 31 and 61.

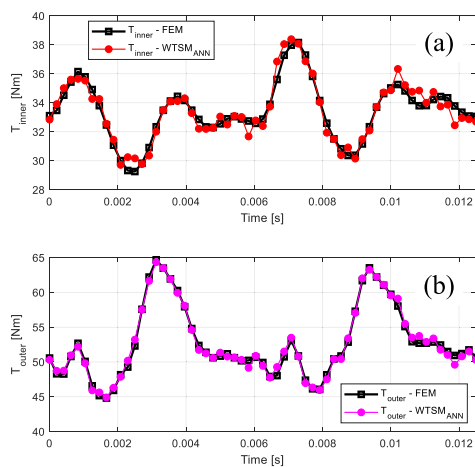


FIGURE 10 Comparison between torque waveforms computed with FEM and WTSM. (a) Inner rotor and (b) outer rotor.

purpose, NSGA II has been adopted since it is more efficient with problems containing large inputs and limited number of objectives. Figure 12a illustrates the results obtained through applying 100 generations and 200 populations size (2×10^4 sample designs in total). In addition, the variation of weight constraint according to studied objectives is illustrated in Figure 12b. Moreover, the movement of NSGA II according to each generation number to find the pareto optimum solutions is shown in Figure 12c. With respect to the extracted pareto front, a final design must be selected according to the application requirements. Moreover, the selected design is a result of surrogate-based optimisation which requires an additional FEM-evaluation to verify the reliability the optimisation result.

4 | COMPARATIVE PERFORMANCE ANALYSIS

Figure 13 shows the obtained optimum design through the proposed ANN-based WTSM and applied NSGA II. However, to comparatively verify the effectiveness of the proposed method, different performance aspects of the obtained pareto solution is analysed in this section.

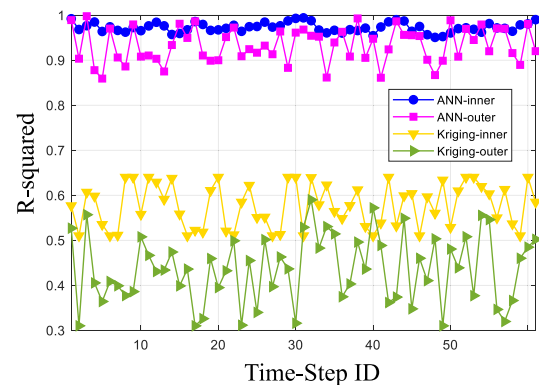


FIGURE 11 Comparison between WTSMs trained with ANN and Kriging.

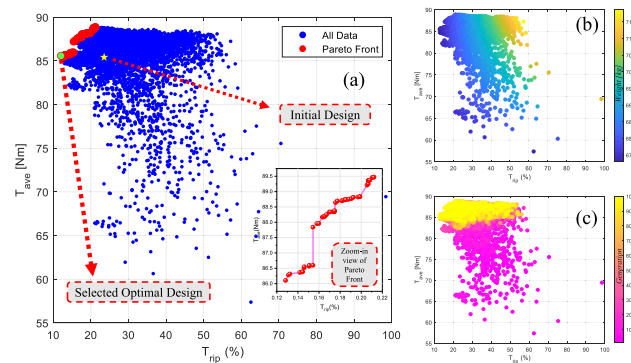


FIGURE 12 Multi-objective optimisation results based on NSGA II. (a) Pareto front, (b) weight distribution and (c) Generation distribution.

4.1 | Electromagnetic performance

Figure 14 shows the comparison between the torque waveform of initial and optimised designs. Also, the obtained performance factors are summarised in Table 3. As can be seen, the average torque has maintained above the defined constraint with a slight improvement. The latter demonstrates the proposed initial design technique in phase 1 effectively provided a good starting point in terms of maximising the torque density. However, the torque ripple reduced from 23.61% to 10.62%. By analysing the harmonic orders of torque waveforms through fast Fourier transformation (FFT), it is evident that three major harmonic amplitudes are compensated leading to a much smoother operating torque in the optimised DSS-DRSynRM (see Figure 15). The shape variation for torque waveform of inner and outer rotors are reported in Figure 16. Further comparative investigation on torque waveform of each rotor segments proves that the applied optimisation algorithm was able to create a phase difference near to 180 electrical degrees with the three most significant harmonics frequencies (160 Hz, 320 and 480 Hz). Therefore, a destructive interference has been occurred to reduce the resultant harmonic amplitude in the output torque of the optimised DSS-

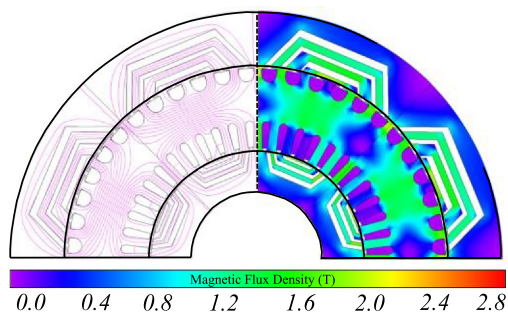


FIGURE 13 The optimal design with the proposed method.

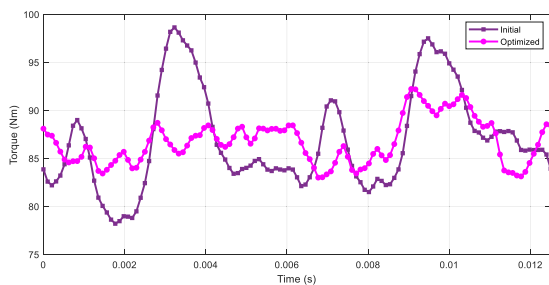


FIGURE 14 Optimised versus initial torque waveforms of DSS-DRSynRM.

TABLE 3 Performance comparison results.

Design	T_{ave} (Nm)	T_{rip} (%)	Weight (kg)
Initial	86.53	23.61	70.168
Optimised	86.748	10.62	68.66

DRSynRM. Thanks to the availability of all 26 design variables for the optimisation, it was possible to simultaneously modify the torque waveforms of each segment according to each other leading to the minimised torque ripple while maximising the average torque. The obtained optimum design also presents an improved performance considering field weakening (FW) operation and increased current angle with respect to the maximum torque per ampere (MTPA) point. As it is illustrated in Figure 17, while both designs provide a similar average torque, the variation range of torque pulsation is considerably lower with the optimised DSS-DRSynRM. The latter can also be considered as an indirect benefit of proposed optimal design method.

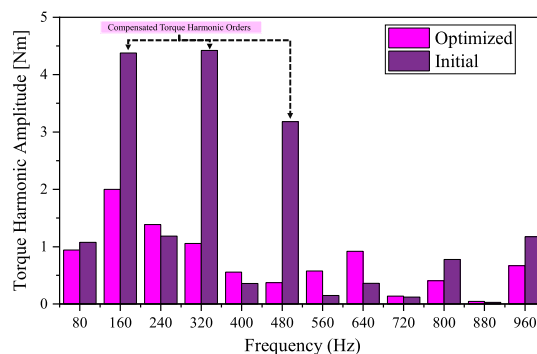


FIGURE 15 Harmonic comparison of initial and optimised torque waveforms using FFT.

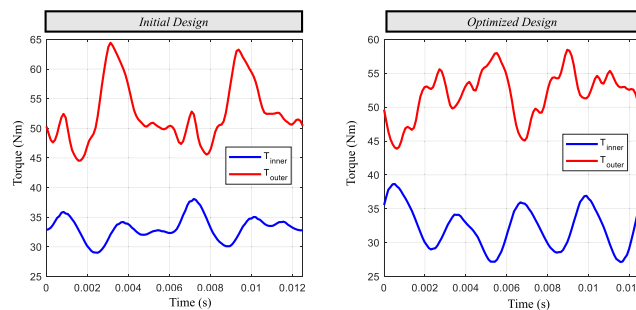


FIGURE 16 Inner and outer rotor torque waveforms for initial and optimised designs.

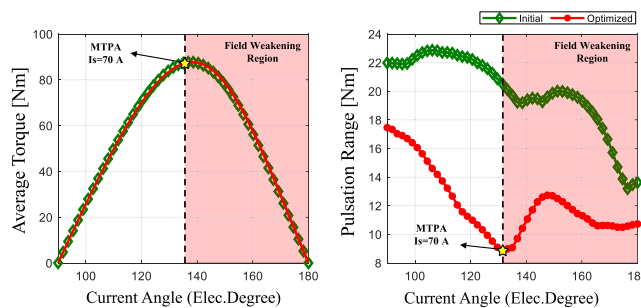


FIGURE 17 Performance versus current angle: (a) average torque and (b) pulsation range.

4.2 | Computational efficiency

To computationally validate the effectiveness of the proposed ANN-based WTSM and torque waveform decomposition method, the same problem has been solved using a very popular surrogate-based multi-level approach used for variety of electrical machine optimisation problems [21]. Figure 18 shows the applied multi-level optimisation where the design space has been divided to 2 levels. Each level represents 13 variables regarding a specific rotor segment. For example, in first level, the design parameters of outer rotor are fixed at their initial value. Meanwhile, the design parameters located on the inner rotor will be optimised to minimise the torque ripple and maximise the average torque. After finishing this stage, the best optimum solution will be selected for the next level. At second step, the same procedure will be followed for optimising outer rotor design parameters while the inner rotor will remain fixed. The algorithm will repeat itself until the convergence is achieved by minimising the cost function (f_{\min}) in each pareto front. The utilised cost function is written as follows:

$$f_{\min} = \frac{T_{\text{ave}}}{T_{\text{ave-initial}}} + \frac{T_{\text{rip}}(\%)_{\text{initial}}}{T_{\text{rip}}(\%)} \quad (6)$$

Each level consists of 13 variables. In this regard, an adequate number of samples needs to be generated for construct surrogate models with appropriate accuracy in each level. As the total FEM simulations for proposed method was 1000 for inner rotor and 4000 for outer rotor, the same amounts also have been considered for minimum initial dataset. However, due to sensitive nature of $T_{\text{rip}}(\%)$ and large number of variables, the datasets has increased to 3000 samples and 5000 samples, respectively.

Figure 19 illustrates the optimisation samples and pareto front generated in different levels. As can be seen, each level has resulted in a different pareto front and minimised cost function. Table 4 summarises the optimum values obtained in

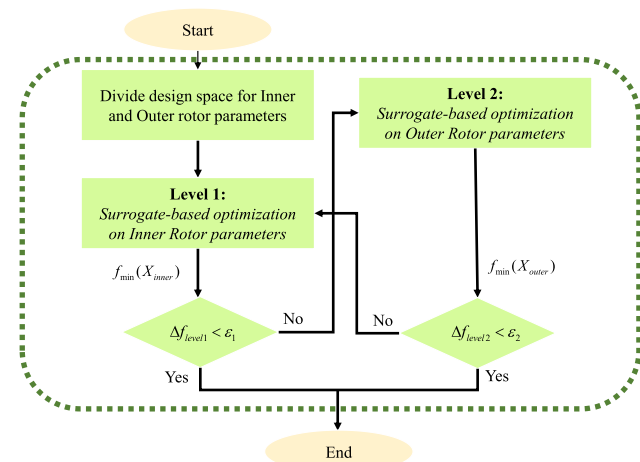


FIGURE 18 Multi-level optimisation flowchart for DSS-DRSynRM.

each pareto front. Moreover, the measured cost function is also included for comparison purposes. It is evident that the proposed method has been able to provide a lower cost function with 37.5% reduction in the required number of FEM simulations for the optimisation of DSS-DRSynRM. This parallel improvement in computational efficiency demonstrates the superiority of the proposed method in comparison with the existing multi-level approach.

5 | CONCLUSION

A new high-dimensional optimal design method for DSS-DRSynRMs based on the combination of data-driven models and torque waveform decomposition feature was presented in this article. The proposed method was structured into three distinct phases to enhance computational efficiency and design accuracy. In the first phase, it has been demonstrated that an optimal initial sizing of the stator yoke enables the decoupling of the magnetic interaction between the inner and outer rotors. By establishing the principle of torque waveform decomposability DSS-DRSynRMs, the design space was partitioned into smaller independent subspaces, significantly reducing the computational complexity of the optimisation process. In the second phase, the application of a newly proposed WTSM strategy for optimisation of DSS-DRSynRMs is comprehensively studied. By means of combining WTSM with ANN, two improvements are achieved:

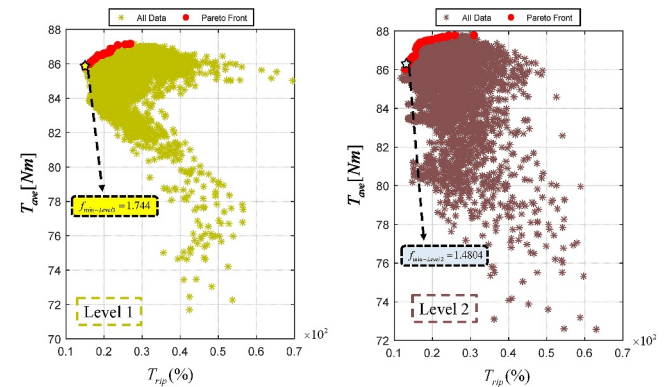


FIGURE 19 Multi-level optimisation based on NSGA II. (a) Level 1 and (b) Level 2.

TABLE 4 Summarised optimisation results with multi-level and proposed methods.

Case	Number of Variables	T_{ave} (Nm)	T_{rip} (%)	Weight (kg)	f_{\min}
Multilevel-8000 FEM	Level 1 (13 variables)	86.19	17.4	71.14	1.7440
	Level 2 (13 variables)	86.39	11.3	69.37	1.4802
Proposed-5000 FEM	26 variables	86.748	10.62	68.22	1.4523

- (1) Applied WTSM strategy allowed to simultaneously model and optimise both rotor segments. The latter is not possible with the conventional approaches such as multi-level optimisation.
- (2) Employing ANN over traditional fitting techniques such as kriging improved the accuracy. Also reduced the need for extensive FEM simulations for surrogate models particularly in high-dimensional problems.

At the last phase, the pareto solutions alongside the optimal design were found using NSGAI.

In order to evaluate the effectiveness of the proposed method, the electromagnetic and computational efficiency aspects were analysed showing a superior performance compared to initial design and multi-level method, respectively.

AUTHOR CONTRIBUTIONS

Farnam Farshbaf-Roomi: Formal analysis; Software, Visualisation. **Aran Shoaie:** Investigation; Methodology; Validation. **Jianguo Zhu:** Data curation; Project administration; Supervision. **Qingsong Wang:** Resources; Supervision; Writing—original draft

ACKNOWLEDGEMENTS

This research is supported by the Natural Sciences and Engineering Research Council of Canada.

CONFLICT OF INTEREST STATEMENT

There are no conflicts of interest between the authors of the presented manuscript.

DATA AVAILABILITY STATEMENT

The data that support the findings of this study are available from the corresponding author upon reasonable request.

ORCID

Farnam Farshbaf-Roomi  <https://orcid.org/0009-0008-4524-0426>

Aran Shoaie  <https://orcid.org/0009-0006-3502-3327>

REFERENCES

1. Guo, X., et al.: Design and analysis of a novel synthetic slot dual-PM machine. *IEEE Access* 7, 29916–29923 (2019). <https://doi.org/10.1109/ACCESS.2019.2902460>
2. Zhao, W., et al.: Dual airgap stator- and rotor-permanent magnet machines with spoke-type configurations using phase-group concentrated coil windings. *IEEE Trans. Ind. Appl.* 53(4), 3327–3335 (2017). <https://doi.org/10.1109/TIA.2017.2681618>
3. Baloch, N., et al.: Low-cost dual-mechanical-port dual-excitation machine for washing machine application. *IEEE Access* 7, 87141–87149 (2019). <https://doi.org/10.1109/ACCESS.2019.2926302>
4. Yeh, Y.H., Hsieh, M.F., Dorrell, D.G.: Different arrangements for dual-rotor dual-output radial-flux motors. *IEEE Trans. Ind. Appl.* 48(2), 612–622 (2012). <https://doi.org/10.1109/TIA.2011.2180495>
5. Zhang, Z., et al.: Electromagnetic and structural design of a novel low-speed high-torque motor with dual-stator and PM-reluctance rotor. *IEEE Trans. Appl. Supercond.* 30(4), 1–5 (2020). <https://doi.org/10.1109/TASC.2020.2977286>
6. Li, Y., Bobba, D., Sarlioglu, B.: Design and optimization of a novel dual-rotor hybrid PM machine for traction application. *IEEE Trans. Ind. Electron.* 65(2), 1762–1771 (2018). <https://doi.org/10.1109/TIE.2017.2739686>
7. Alani, M., et al.: Analysis and design of dual-rotor synchronous reluctance machine. *IEEE J. Emerg. Sel. Top. Power Electron.* 9(4), 4376–4383 (2021). <https://doi.org/10.1109/JESTPE.2020.3047404>
8. Shoaie, A., Wang, Q.: A comprehensive review of concentric magnetic gears. *IEEE Trans. Transp. Electr.* 10(3), 1–5598 (2023). <https://doi.org/10.1109/TTE.2023.3317772>
9. Shoaie, A., Wang, Q.: A high torque density flux-focusing halbach magnetic gear for electric vehicle applications. In: 2022 IEEE 1st Industrial Electronics Society Annual On-Line Conference (ONCON), pp. 1–6 (2022). <https://doi.org/10.1109/ONCON56984.2022.10126858>
10. Bramerdorfer, G., et al.: Modern electrical machine design optimization: techniques, trends, and best practices. *IEEE Trans. Ind. Electron.* 65(10), 7672–7684 (2018). <https://doi.org/10.1109/TIE.2018.2801805>
11. Xie, B., et al.: Rotor multidisciplinary optimization of high speed PMSM based on multi-fidelity surrogate model and gradient sequential sampling. *IEEE Trans. Energy Convers.* 38(2), 859–868 (2023). <https://doi.org/10.1109/TEC.2022.3214992>
12. Gu, J., et al.: Surrogate model-based multiobjective optimization of high-speed PM synchronous machine: construction and comparison. *IEEE Trans. Transp. Electr.* 9(1), 678–688 (2023). <https://doi.org/10.1109/TTE.2022.3173940>
13. Lei, G., et al.: Robust design optimization of electrical machines: a comparative study and space reduction strategy. *IEEE Trans. Energy Convers.* 36(1), 300–313 (2021). <https://doi.org/10.1109/TEC.2020.2999482>
14. Im, S.Y., et al.: Kriging surrogate model-based design of an ultra-high-speed surface-mounted permanent-magnet synchronous motor considering stator iron loss and rotor eddy current loss. *IEEE Trans. Magn.* 58(2), 2–6 (2022). <https://doi.org/10.1109/TMAG.2021.3080119>
15. Jin, R., Chen, W., Sudjianto, A.: On sequential sampling for global metamodeling in engineering design. *International design engineering technical conferences and computers and information in engineering conference* 36223, 539–548 (2002)
16. Farshbaf Roomi, F., Vahedi, A., Mirnikjoo, S.A.: Multi-objective optimization of permanent magnet synchronous motor based on sensitivity analysis and Latin hypercube sampling assisted NSGAI. In: 2021 12th Power Electron. Drive Syst. Technol. Conf. PEDSTC 2021, pp. 1–5 (2021). <https://doi.org/10.1109/PEDSTC52094.2021.9405918>
17. Li, Y., et al.: Machine learning for design optimization of electromagnetic devices: recent developments and future directions. *Appl. Sci.* 11(4), 1627 (2021). <https://doi.org/10.3390/app11041627>
18. Im, S.-Y., et al.: Kriging surrogate model-based design of an ultra-high-speed surface-mounted permanent-magnet synchronous motor considering stator iron loss and rotor eddy current loss. *IEEE Trans. Magn.* 58(2), 1–5 (2021). <https://doi.org/10.1109/tmag.2021.3080119>
19. Shoaie, A., Farshbaf-Roomi, F., Wang, Q.: Surrogate-based multi-objective optimization of flux-focusing halbach coaxial magnetic gear. *Energies* 17(3), 608 (2024). <https://doi.org/10.3390/en17030608>
20. Farshbaf Roomi, F., Vahedi, A., Nobahari, A.: Electrical machines surrogate-based design optimization based on novel waveform targeting strategy with improvement of the computational efficiency. *IET Electr. Power Appl.* 16(11), 1286–1299 (2022). <https://doi.org/10.1049/elp2.12226>
21. Sun, X., et al.: Multi-objective design optimization of an IPMSM based on multilevel strategy. *IEEE Trans. Ind. Electron.* 68(1), 139–148 (2021). <https://doi.org/10.1109/TIE.2020.2965463>

How to cite this article: Farshbaf-Roomi, F., et al.: High-dimensional optimal design of dual-rotor synchronous reluctance machines based on data-driven torque decomposition. *IET Electr. Power Appl.* e12535 (2025). <https://doi.org/10.1049/elp2.12535>